Am J Physiol Heart Circ Physiol 291: H1670–H1678, 2006.
First published May 19, 2006; doi:10.1152/ajpheart.00097.2006.

Wave reflection effects in the central circulation of American alligators (*Alligator mississippiensis*): what the heart sees

Douglas A. Syme,[1] A. Kurt Gamperl,[2] Marvin H. Braun,[3] and David R. Jones[3]

[1]*Department of Biological Sciences, University of Calgary, Calgary, Alberta;* [2]*Ocean Sciences Centre, Memorial University of Newfoundland, St. John's, Newfoundland; and* [3]*Department of Zoology, University of British Columbia, Vancouver, British Columbia, Canada*

Submitted 23 January 2006; accepted in final form 12 May 2006

Syme, Douglas A., A. Kurt Gamperl, Marvin H. Braun, and David R. Jones. Wave reflection effects in the central circulation of American alligators (*Alligator mississippiensis*): what the heart sees. *Am J Physiol Heart Circ Physiol* 291: H1670–H1678, 2006. First published May 19, 2006; doi:10.1152/ajpheart.00097.2006.—A large central compliance is thought to dominate the hemodynamics of all vertebrates except birds and mammals. Yet large crocodilians may adumbrate the avian and mammalian condition and set the stage for significant wave transmission (reflection) effects, with potentially detrimental impacts on cardiac performance. To investigate whether crocodilians exhibit wave reflection effects, pressures and flows were recorded from the right aorta, carotid artery, and femoral artery of six adult, anesthetized American alligators (*Alligator mississippiensis*) during control conditions and after experimentally induced vasodilation and constriction. Hallmarks of wave reflection phenomena were observed, including marked differences between the measured profiles for flow and pressure, peaking of the femoral pressure pulse, and a diastolic wave in the right aortic pressure profile. Pulse wave velocity and peripheral input impedance increased with progressive constriction, and thus changes in both the timing and magnitude of reflections accounted for the altered reflection effects. Resolution of pressure and flow waves into incident and reflected components showed substantial reflection effects within the right aorta, with reflection coefficients at the first harmonic approaching 0.3 when constricted. Material properties measured from isolated segments of blood vessels revealed a major reflection site at the periphery and, surprisingly, at the junction of the truncus and right aorta. Thus, while our results clearly show that significant wave reflection phenomena are not restricted to birds and mammals, they also suggest that rather than cope with potential negative impacts of reflections, the crocodilian heart simply avoids them because of a large impedance mismatch at the truncus.

blood pressure; blood flow; impedance; pulse wave velocity; harmonics

BLOOD EJECTED DURING ventricular systole enters the central arteries and creates pressure and flow waves as it travels toward the peripheral circulation. These waves are then reflected back toward the heart when they encounter impedance mismatches due to tapering, altered compliance, or local discontinuities (8, 12, 16, 23, 24, 28, 30). While reflections originate to some extent along the entire length of the arterial system (32), it is the high impedance of arterial terminations that are the major sites of reflections (8, 23, 28, 37). As such, reflections tend to be increased by constriction and decreased by dilation of the vascular beds (30). The resultant waves in blood vessels are composed of a forward wave generated by cardiac ejection and a series of progressively damped incident and reflected waves (5), although in practice the waves are typically resolved into single forward and reflected composites. Pressure waves are reflected in phase, whereas the flow wave is reflected out of phase, and thus as the reflected components travel back toward the heart, they interfere with forward traveling components and result in local enhancement of pressure (peaking or amplification) and local reductions in flow (12, 24, 28). In combination, ventricular ejection, the pulse wave velocity, and the magnitude and timing of the reflections determine the resultant flow and pressure profiles in the circulation (5, 23).

The location of the heart within this reflecting system will influence the load that it must work against and impedance coupling between the heart and the arterial system (8, 9, 28). This location and its impact on cardiac performance are related to the distance of the heart from the reflecting sites, the pulse wave velocity, and the time course of the cardiac cycle (12, 28). In healthy, young mammals in which it has been studied, the main reflected pressure wave tends to return during early diastole, resulting in a diastolic "wave" or "hump" that enhances coronary perfusion. However, with arterial stiffening, the pulse wave velocity increases and the reflections return during late systole, resulting in an increased systemic pressure and an increased load against which the heart must work (23, 24, 27, 28). Thus the timing and magnitude of the reflections have important implications for cardiovascular function, and correlations have been found between the timing of return to the heart of reflected waves, the resultant amplification of the pressure pulse during systole, and the risk of coronary heart disease (11, 35). The significance of appropriate timing of wave reflections at the heart has even been implicated as being responsible for the inverse relationship between animal size and heart rate (20), although Jones (13) contends that the specific location of the heart within the reflecting system does not scale as might be expected if this were a critical design element, and other constraints on the design of the vascular tree are suggested (15).

With the exception of birds and mammals, wave transmission effects are probably of little consequence for vertebrates, where a large central compliance dominates their hemodynamics, and most tend to be small with relatively short arterial systems (7, 13, 16). However, in larger, elongate reptiles, such as crocodilians or snakes, the long pulse transit times and relatively slow heart rates may predispose them to considerable

Address for reprint requests and other correspondence: D. A. Syme, Dept. of Biological Sciences, Univ. of Calgary, 2500 Univ. Dr. NW, Calgary, Alberta, T2N 1N4, Canada (e-mail: syme@ucalgary.ca).

The costs of publication of this article were defrayed in part by the payment of page charges. The article must therefore be hereby marked "*advertisement*" in accordance with 18 U.S.C. Section 1734 solely to indicate this fact.

reflection effects at the heart (13). Wave reflections have been recorded in diamond pythons, yet a concomitant increase in the pulse wave amplitude toward the periphery is not observed (1). This lack of amplification appears to be due to *1*) the relatively uniform distribution of peripheral reflecting sites in the limbless architecture of snakes, compared with a more discrete apparent reflecting site at limb bifurcations in most other animals (1); and *2*) perhaps an interaction between elastic nonuniformity of the vessels and viscous damping (2).

Although crocodilians have slow heart rates and elongate bodies like snakes, they also possess limbs and thus probably exhibit a reflection pattern that is more typical of mammals and birds. This suggests that they may show pronounced wave transmission properties and perhaps significant reflection effects at the heart that, in turn, may enhance or degrade cardiac performance. Because of the interactions between natural changes in heart rate, vascular impedance, and indeterminate growth patterns that result in a wide range of body lengths over their normal life span, these large reptiles may be exposed to extreme challenges with regard to managing the potentially negative impacts of wave reflection effects at the heart. Therefore, the goals of this study were *1*) to measure pressure and flow profiles in the central and peripheral circulation of American alligators to assess whether they experience significant reflection effects; *2*) to use the material properties of isolated segments of central and peripheral blood vessels to reveal the basis for, and site of, potential reflections; and *3*) to establish how the reflections might impact cardiac function in these animals.

In the crocodilian heart (Fig. 1), the left ventricle gives rise to the truncus that gives rise in turn to the right systemic aorta which serves as the only systemic trunk when the heart operates in the avian mode, whereas the right ventricle gives rise to the pulmonary arteries and to a left systemic aorta, the latter also serving the systemic circulation in reptilian mode (14). In the present study, the occurrence of pressure and flow wave reflections were assessed in the right aorta, ~10 cm distal to the heart, near the right subclavian artery. This specific site was selected because the right aorta is the primary systemic vessel and the location is convenient, yet close enough, to the heart to infer wave reflection effects approaching the heart itself. Material properties were then measured from isolated segments of the truncus, the proximal and distal right aorta, proximal and distal carotid artery, and femoral artery (Fig. 1), these vessels being selected for resolution of the site(s) of reflection in the vascular tree.

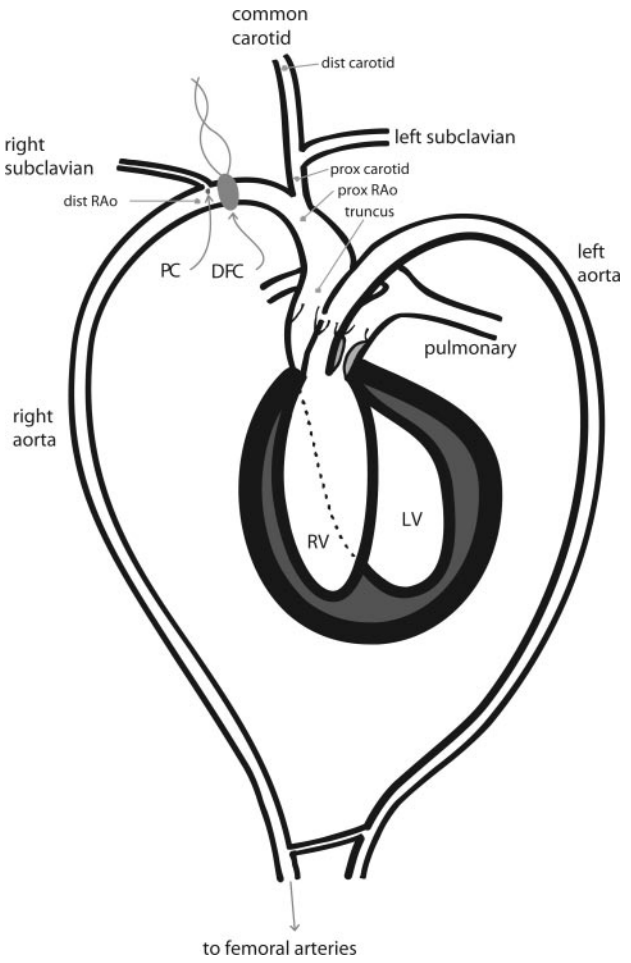

Fig. 1. Representative drawing of crocodilian heart and central circulation showing approximate locations of recordings and sites of vessel samples. Right aortic Doppler flow cuff (DCF), right aortic pressure catheter (PC), and vessel samples classified as distal carotid (Dist carotid), proximal carotid (Prox carotid; DFC was placed on carotid artery near this location), distal right aorta (Dist RAo), proximal right aorta (Prox RAo), and truncus are shown. Vessel samples and pressure recordings were also taken from left femoral artery ~10 cm distal to its bifurcation at termination of RAo (not shown on figure). RV and LV, right and left ventricle, respectively.

MATERIALS AND METHODS

Animals. All animal husbandry and experimental procedures were approved by the Institutional Animal Care and Use Committee at the University of British Columbia. Young American alligators (*Alligator missippiensis*, Daudin) were obtained from commercial farms in Florida and held in the University's animal care facilities for approximately five years until they reached an appropriate size. The alligators were housed individually or in small groups in rooms (~15 m^2) maintained at 30°C and that contained a shallow pool in which they could submerge. They were fed commercial dog chow ad libitum and given chopped chicken and vitamin supplements weekly. All animals were growing and appeared healthy before the experiments.

Anesthesia and instrumentation. Details of sedation, exposure of the central vasculature, pressure catheter preparation and measurement procedures, and nonocclusive catheterization of the right subclavian artery have been described previously (34). One catheter was placed in the right subclavian artery, which branches directly off of the right aorta about 10 cm distal to the heart, and was fed centrally until the tip lay near the junction with the right aortic arch (Fig. 1); this catheter was used to monitor central arterial (i.e., right aortic) blood pressure. The catheter was ~20 cm long and had a frequency response of 11 Hz. A second catheter was placed in the left femoral artery and was used to monitor peripheral pressure at this location. The distance between the tips of the femoral and aortic pressure catheters was determined by directly measuring the length of the vessels through the exposed thorax (postexperimentally) and approximating the remaining distance from the abdomen to the tip of the catheter in the leg. Average pulse wave velocity was calculated by dividing this distance by the difference in time between arrival of the foot of the pressure waves at the two recording sites. There are conflicting reports as to the effects of heart rate on pulse wave velocity (17, 38), so velocity was calculated separately in each animal and at each state of control, vasodilation, or vasoconstriction (see *Recordings and data analysis* below).

Close-fitting, pulsed Doppler flow cuffs (4–8 mm diameter, Iowa Doppler Products, Iowa City, IA) were placed around the right aorta near the subclavian junction and around the common carotid artery

(Fig. 1) and connected to a Directional Pulsed Doppler Flowmeter (model 545C-4, Bioengineering University of Iowa). Pressure and flow in the right aorta were used to calculate central impedance and reflection phenomena in the central circulation near the heart (described in *Recordings and data analysis*). The precise separation between the right aortic flow cuff and pressure catheter was not measured, but the distance was very small relative to the wavelength of the pulse (range 4–8 m), and so errors in calculation of impedance modulus, as a result of assuming zero separation between recording sites, would be small and can be ignored (36). Flow in the carotid artery was used in conjunction with pressure in the right aorta to approximate peripheral resistance and impedance. This assumes that right aortic pressure is indicative of carotid pressure. Inaccuracies resulting from this assumption are not critical as peripheral resistance/impedance are not required to evaluate reflection effects in the central circulation; they were only used as a qualitative estimate of changes in the extent of dilation/constriction.

The electronics in the pulsed Doppler flowmeter incorporate a single-pole, low-pass resistance-capacitance filter on the analog output with a −3-dB point of 15 Hz. Mitchell et al. (22) have shown that errors in calculating flow moduli and thus impedance due to attenuation caused by flowmeter filters become significant only as the spectrum approaches the cutoff frequency of the filter. Because the cutoff frequency of the filter was about an order of magnitude higher than the lower harmonics analyzed and about triple the frequency of the higher harmonics analyzed, its effects on signal amplitude would be very small and were ignored. The filter also caused a small frequency-dependent phase shift in the flow signals of ~0.03 rad. We used specifications provided by the manufacturer of the flowmeter to calculate and correct for the phase shifts in the flow signals at each frequency that they were measured.

The flow signals were calibrated after each experiment by removing the segments of the vessels to which the cuffs were attached and forcing blood through the vessels at controlled rates with a peristaltic pump while monitoring the signal from the flow meter. Pressure transducers were calibrated routinely during experiments against a mercury column.

Recordings and data analysis. Measurements were made from six animals. Blood pressure and flow were recorded at 166 Hz on a computer using Labtech Notebook Pro v9.0 software (Labtech, Andover, MA). This collection rate exceeds, by over 30-fold, the highest frequency at the highest harmonic analyzed in any animal. One- to two-minute sequences of blood flow and pressure were measured from animals in control states (which were baseline vasodilated due to the anesthetic), after vasodilation (administration of 1 μg/kg isoproterenol into an infusion catheter in the femoral vein), and after vasoconstriction (administration of 20 μg/kg phenylephrine through the infusion catheter). These doses were sufficient to induce the desired effect (see RESULTS) yet allowed the animal to recover from the drug within 10–20 min.

Wave reflections were calculated from the time domain signals according to Li (19) and based on established principles (24, 25, 37). We chose this method because it is computationally simple, can be applied directly to the time domain signals, and is functionally equivalent to and provides results similar to frequency domain analysis and method of characteristics analysis (18, 19, 31). With the use of this analysis, the measured pressure and flow signals could be resolved into incident (forward) and reflected components based on the characteristic impedance (Z_c) of the central circulation. Z_c was calculated as the ratio of pressure to flow obtained from the early portion of the upstroke in systole, before reflections can return to the heart (18, 19, and references therein) as follows. For each animal in each state (control, vasoconstriction, and vasodilation), a series of 10–16 pairs of flow and pressure gradients were measured during the upstroke portion of early systole from each heartbeat in a sequence, for a total of 150–550 data pairs for each animal in each state. From each data pair, the ratio of pressure to flow was calculated and plotted versus the pressure gradient. The plots were then fitted with an exponential rise equation, and the asymptote was taken as Z_c for that particular animal and state. As confirmation, input impedance was calculated at the third harmonic (Z_3) using Fourier analysis; at high harmonics the amplitude of wave reflections are trivial and the wavelength is too short to allow significant reflections at the site of origin, so the input impedance (Z_3) should approximate Z_c (18, 22, 37). Whereas a higher harmonic would be preferable, the third harmonic was used because in some cases the signal amplitude at higher harmonics could not be resolved with confidence. The ratio of Z_c to Z_3 was 1.07 ± 0.075 (±SE) across all animals and states and was not significantly different from 1 ($P = 0.357$), confirming that our calculations of Z_c appear consistent and reliable. In contrast, the average ratio of Z_c to Z_0 (where Z_0 is the input resistance or mean ratio of pressure to flow) was 0.14 ± 0.026 (±SE), foreshadowing the existence of wave reflection effects in these animals. All time domain calculations were applied to the signals using AcqKnowledge software (v3.01, BIOPAC Systems, Santa Barbara, CA).

In addition, Fourier analysis was used to study the frequency spectrum of impedance moduli, phase, and reflection coefficients according to Westerhof et al. (37) and Laskey and Kussmaul (18). Spectra were calculated from analysis of ~10 consecutive beats to reduce noise in the signal (23). The fundamental (zero order or mean) and first four to five harmonics of pressure and flow were determined by using the Fourier analysis routine in LabView 5.1 (National Instruments, Austin, TX), which provided the root mean square amplitude and phase (radians) frequency spectra from a time-domain signal. From these, the input impedance moduli (Z_n) and phase (pressure-flow) were calculated at each harmonic (n). The global reflection coefficient, which describes the relative magnitude of the reflection at the recording site, was calculated at each harmonic as $(Z_n - Z_c)/(Z_n + Z_c)$ (18, 19).

Material properties of blood vessels. Material properties were examined in blood vessels dissected postmortem, including the femoral artery ($n = 3$), right aorta ($n = 5$), carotid artery ($n = 5$), and the truncus chamber serving the right aorta ($n = 5$) (Fig. 1). Proximal and distal regions of the carotid and right aorta were tested separately. Tissue classified as proximal carotid was located 3 cm distal to its bifurcation with the right aorta, whereas distal carotid sections were located 10–13 cm distal to the bifurcation. The proximal right aorta was immediately distal to the truncus, and distal right aorta was at least 10 cm distal to the truncus (similar to the location at which pressures and flows were recorded). Vessel segments were sectioned, forming loops, and arterial dimensions and force-extension properties were measured following methods described by Braun et al. (6). Modifications to the described methods included measurement of wall thickness of the vessels to ±0.001 mm, use of an Instron testing machine (Instron, Norwood, MA) to measure uniaxial force-extension characteristics, a test temperature of 20°C, and force-extension tests performed by cyclic stretching at 3 cm/min. Vessel wall strain (ϵ), true stress (σ), and circumferential stiffness (incremental modulus, E_{inc}) were calculated as described previously (4, 6) and used to calculate pulse wave velocity (c_o), Z_c, and reflection ratios according to Milnor (21). The reflection ratio between the distal right aorta and femoral arteries was calculated with the assumption that the femoral arteries present an impedance equivalent to two vessels in parallel. Strains for these calculations were estimated from a single set of arterial inflations of the right aorta, carotid artery, and femoral artery, performed as in Braun et al. (6); the truncus could not be so inflated, so the value from the proximal right aorta was used for calculations. Measurements were based on a blood pressure of 5.5 kPa, similar to that recorded in the anesthetized alligators.

Pressure and flow data at different states of vasoconstriction/vasodilation and harmonics were compared by using one- or two-way repeated-measures ANOVA and Tukey's pairwise comparisons, or paired t-tests where appropriate. Elastic moduli from material properties were compared by using a one-factor ANOVA and a Tukey's

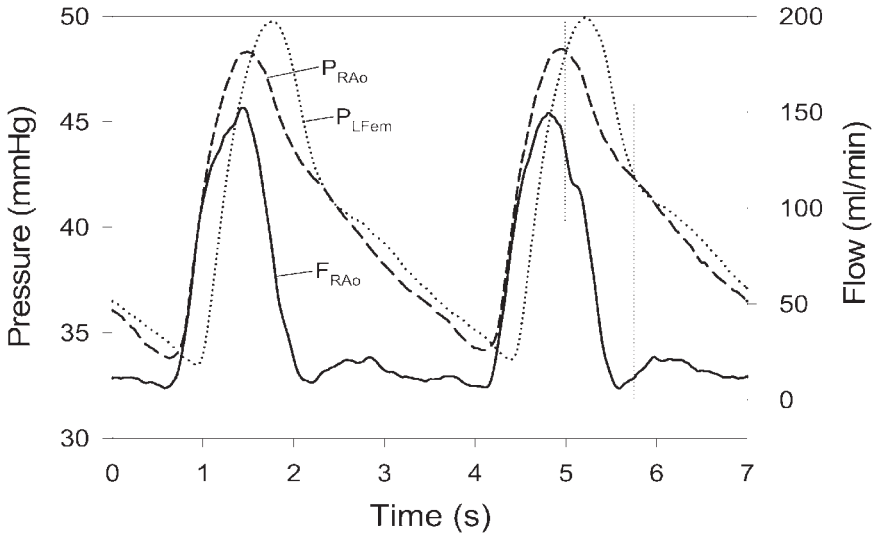

Fig. 2. Pressure profiles in RAo (P_{RAo}) and left femoral artery (P_{LFem}), and flow profile in RAo (F_{RAo}) during two cardiac cycles from an alligator. P_{RAo} and F_{RAo} were measured at a site ~10 cm distal to LV. Vertical dotted lines bound a segment of the records where femoral pressure exceeded aortic pressure.

test. Differences were considered significant at $P < 0.05$. Data in the text and figures are means ± SE.

RESULTS

Pressure and flow profiles. Recordings of flow and pressure were made from six animals: mass, 27.9 ± 4.3 kg, and range, 11–37.7 kg. The distance from the right aortic catheter to the femoral catheter ranged from 47–59 cm and is an estimate of the functional length of the animals in the context of wave reflection effects. Examples of the phase and amplitude relationships for pressure and flow during two cardiac cycles are shown in Fig. 2. Substantial peaking of femoral pressure occurred, to the extent that it exceeded pressure in the right aorta during a considerable portion of late systole and early diastole. In addition, the flow profile measured in the right aorta was markedly different from the pressure profile, a further indication that wave reflections were present.

Heart rate was not affected by the dilation or constriction interventions ($P = 0.336$): control, 31.2 ± 3.2 beats/min; vasodilate, 39.0 ± 3.5 beats/min; and vasoconstrict, 32.4 ± 4.0 beats/min. The onset of the systolic rise of pressure in the right aorta preceded that in the femoral artery (Fig. 2), allowing average pulse wave velocity to be calculated as described in MATERIALS AND METHODS. Pulse wave velocity was significantly faster in animals that were constricted compared with those that were dilated ($P = 0.02$), but constricted and dilated animals were not significantly different from control animals: control, 3.82 ± 0.37 m/s; vasodilate, 2.59 ± 0.22; and vasoconstrict, 4.48 ± 0.29. Mean blood flow in the right aorta was not affected by the state of dilation ($P = 0.68$); however, mean pressure was significantly higher during vasoconstriction and lower during vasodilation ($P < 0.001$) (Fig. 3).

The magnitude of peripheral input resistance (Z_0), as estimated using right aortic pressure and carotid flow, increased to

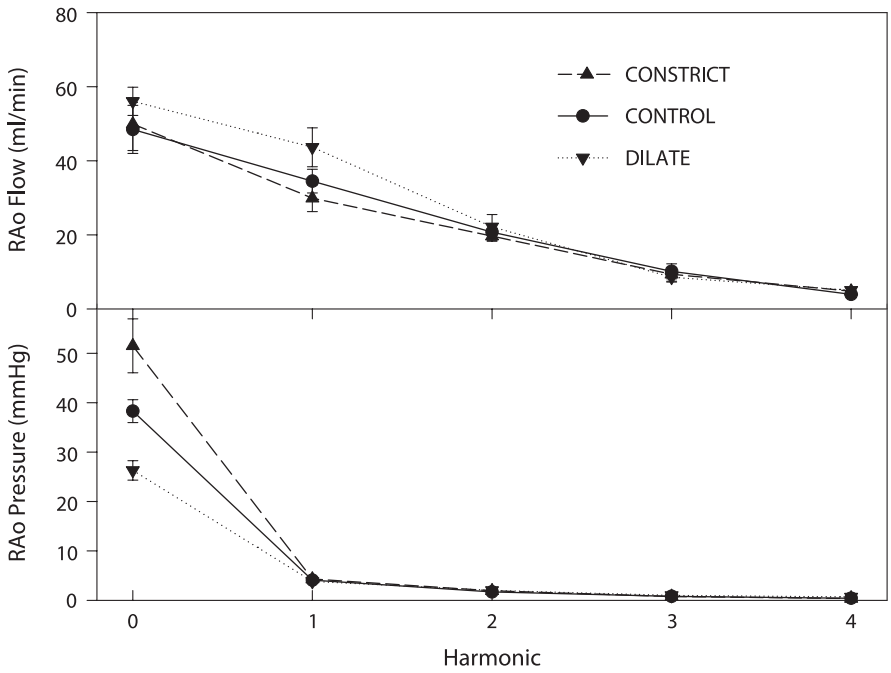

Fig. 3. Mean (0 order) and first 4 harmonics of blood flow (*top*) and pressure (*bottom*) in RAo, measured at a site ~10 cm distal to LV during control conditions, vasodilation, and vasoconstriction. Values are means ± SE; $n = 6$ animals. See RESULTS for statistical description.

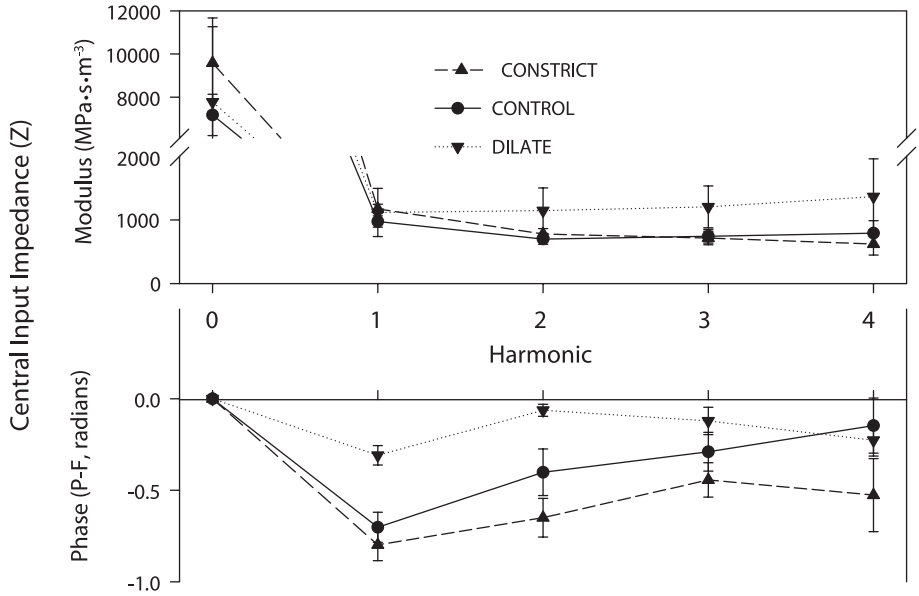

Fig. 4. Modulus (*top*) and phase (*bottom*) of central (RAo) input impedance measured at a site ~10 cm distal to LV during control conditions, vasodilation, and vasoconstriction. Note the break in scale on *y*-axis (*top*). Values are means ± SE; n = 6 animals. See RESULTS for statistical description.

135% of control with vasoconstriction and decreased to 66% of control with vasodilation ($P = 0.021$). Furthermore, this trend was also evident in the moduli of peripheral input impedance from Fourier analysis at the first harmonic ($P = 0.012$), although not at higher harmonics ($P > 0.05$); during vasoconstriction, Z_1 was 192% of that during vasodilation, but the control value was not different from that recorded in constricted or dilated animals. Spectra for peripheral impedance are not shown, because these changes were only used to confirm satisfactory impact of the vasodilatory agents. In contrast to peripheral resistance and impedance, the moduli of central impedance (Z_{1-4}) and central input resistance (Z_0) were not affected by the constriction or dilation interventions ($P = 0.742$) and varied little through *harmonics 1–4* (Fig. 4). The impedance phase was largest at lower harmonics and was significantly smaller in the dilated condition ($P = 0.002$) but did not differ between control and constricted states (Fig. 4). The magnitude of the phase shift was smaller than is typically observed in humans (23), likely due to the higher vessel compliance and slower pulse wave velocity in alligators.

Reflection coefficients were calculated, and time-domain reflection analysis was then performed. In this analysis the global reflection coefficient incorporates the effects of all reflection sources, sites, and magnitudes on a particular point, in this case the recording site in the right aorta. At the first harmonic, the reflection coefficient ranged from near 0 to 0.3, depending on the state of constriction (Fig. 5). Thus up to 30% of the incident wave was effectively reflected back toward the heart when constricted, ~10% during control, but virtually none when dilated. The reflection coefficient was decreased by

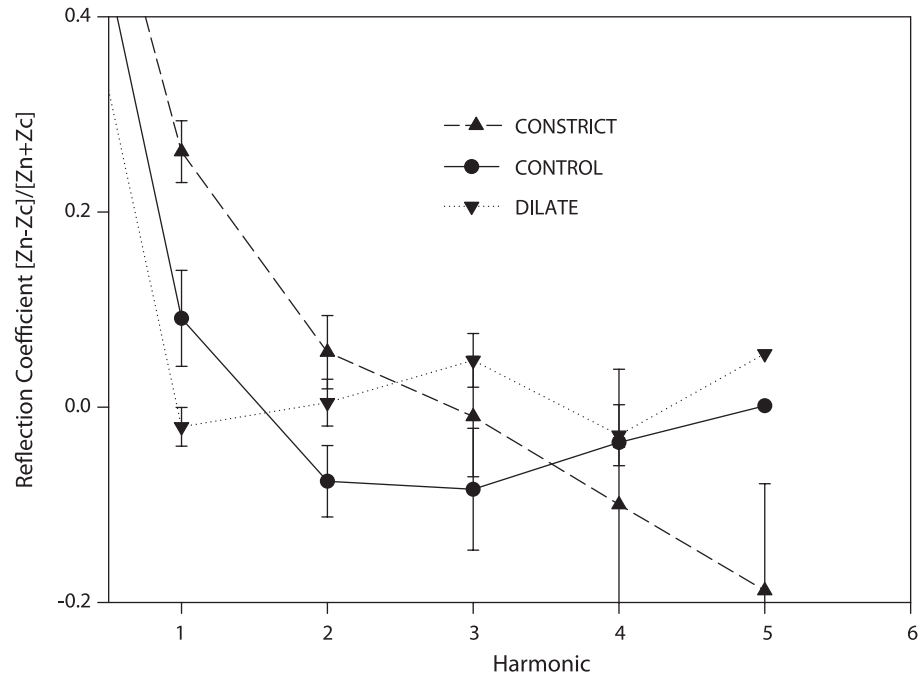

Fig. 5. Global reflection coefficients, measured at right aortic recording site, showing first 5 harmonics during control conditions and after vasodilation and vasoconstriction. Z_n, input impedance moduli; Z_c, characteristic impedance. Values are means ± SE; n = 6 animals. See RESULTS for statistical description.

dilation at the mean ($P = 0.001$) and increased by constriction at the first harmonic ($P < 0.001$) (Fig. 5). This effect is generally similar to that observed in dogs after vasodilation and vasoconstriction (37). The reflection coefficients were relatively small and tended toward zero at higher harmonics.

When the incident and reflected flow and pressure profiles were calculated, a pronounced reflection effect was observed (Fig. 6), similar to that noted in mammals (8). In these analyses only the oscillatory components of the forward and reflected waves are considered; the steady or average pressure and flow components are ignored (37). The magnitude of the reflections in both pressure and flow decreased with dilation and increased with constriction. This resulted in the incident waves most closely matching the measured profiles during the dilated state (small reflection effect) and being most different during the constricted state (large reflection effect). Similarly, the measured flow and pressure profiles were most similar to one another in dilation and least similar when constricted. The

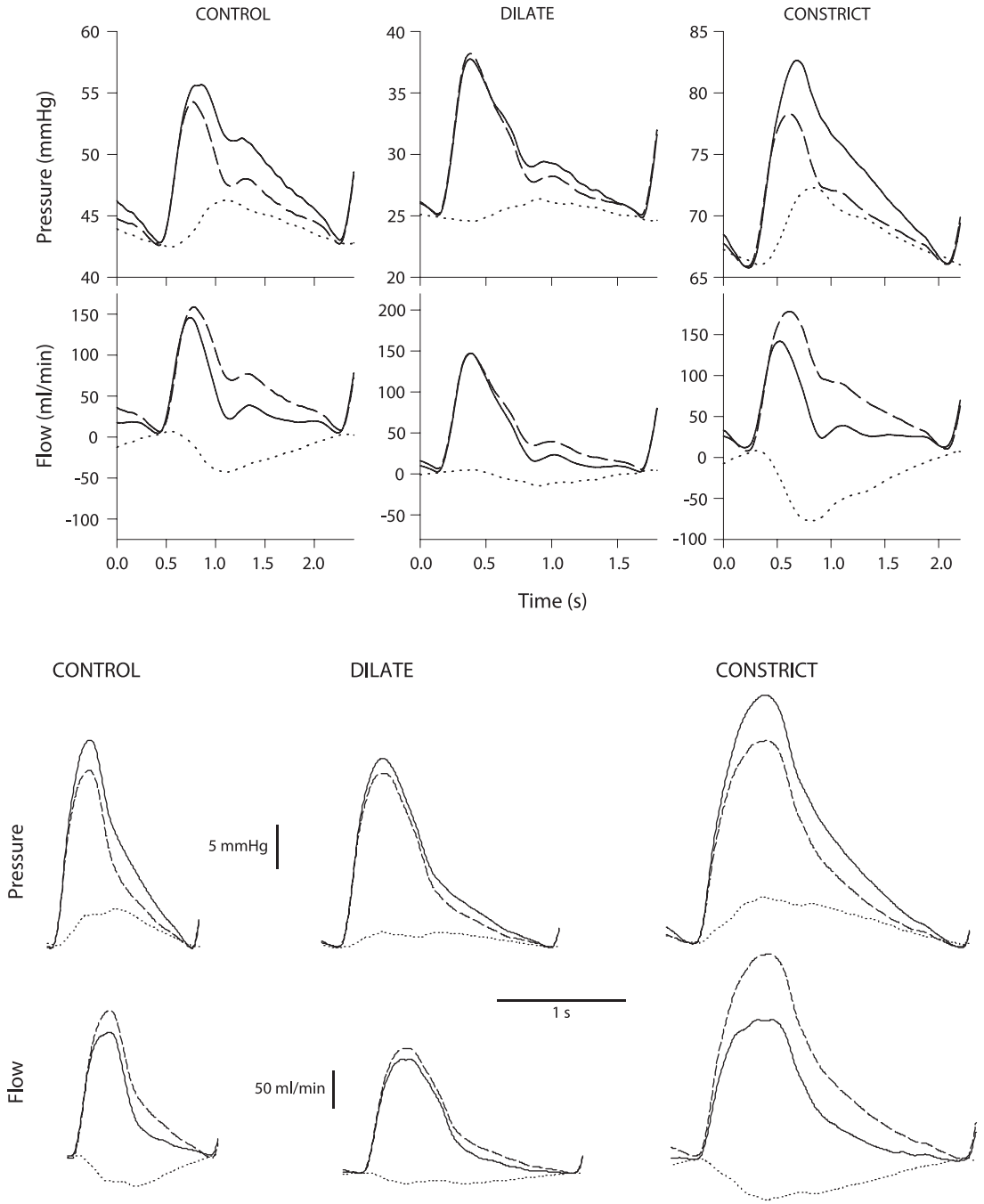

Fig. 6. Pressure and flow profiles at right aortic recording site in 2 animals. Each graph shows measured profile (solid line), incident component (dashed line), and reflected component (dotted line). Steady flow and average pressure terms in component incident and reflected waves are disregarded in these analyses, and thus only magnitude of changes are relevant; incident and reflected waves have been aligned with measured wave at onset of systole only to facilitate comparison. *Top*: graphs representing 1 animal (mass, 37.5 kg) have axes showing absolute pressure and flow. *Bottom*: graphs representing another animal (mass, 11 kg) have scale bars showing magnitude of transients.

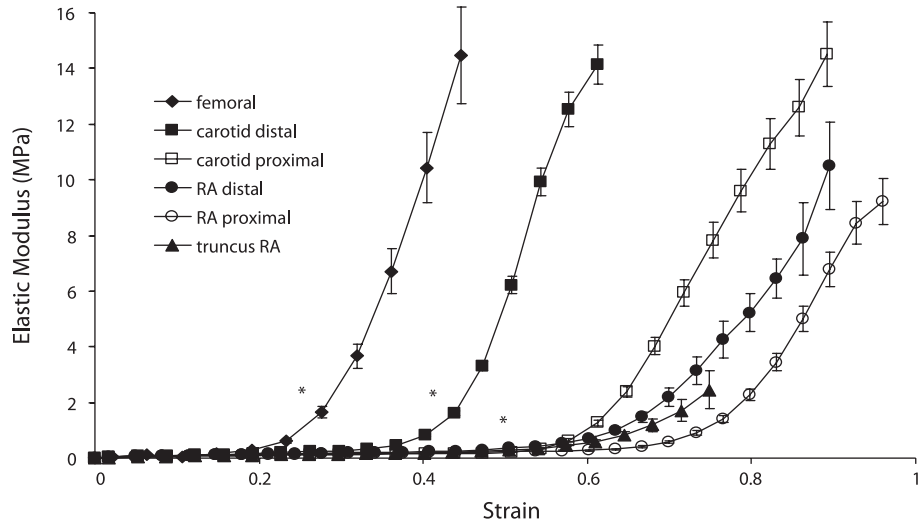

Fig. 7. Elastic modulus-strain relationship for arterial segments from the American alligator. See MATERIALS AND METHODS for precise location of each segment. *Measurements made at physiological strains, based on blood pressure of 5.5 kPa, similar to that recorded in anesthetized animals. RA, right aorta.

large magnitude and early return of the reflected waves in the control and particularly constricted states resulted in *1*) a pronounced prolongation and peaking of the measured central pressure pulse compared with the incident wave and *2*) a pronounced curtailment and notable decrease in the magnitude of the measured flow pulse (Fig. 6). In contrast, during dilation, the reflection was small and arrived well into diastole, resulting in a small diastolic wave but with no affect on the pulse pressure and little effect on incident flow (Fig. 6).

Material properties. The vessels all exhibited the characteristic J-shaped modulus-strain curve of arteries (Fig. 7). However, when compared with central vessels (proximal carotid, right aorta, and truncus), the peripheral vessels (femoral artery and distal carotid) were relatively inextensible and stiff, showing large increases in elastic modulus at relatively small strains. At physiological strains (Table 1 and Fig. 7), the peripheral vessels had similar elastic moduli but remained considerably stiffer than the central vessels. Likewise, there was no significant difference in the modulus-strain characteristics between any of the central vessels at physiological strains (Fig. 7).

The intrinsic pulse wave velocity (c_o) increased moving distally in both the right aorta toward femoral artery and in the carotid artery (Table 1); hence, peripheral pulse wave velocity was significantly faster than central pulse wave velocity. Z_c calculated from material properties varied widely in the alligator vessels, from a low of 12.9 MPa·s·m^{-3} at the truncus/right aorta to 1,279 MPa·s·m^{-3} in the femoral artery (Table 1). The value of Z_c calculated from the material properties of the right aorta and most other central blood vessels (Table 1) was somewhat smaller than the value calculated from measurements of pressure and flow in the right aorta (average, 806 MPa·s·m^{-3} under control conditions).

Reflection ratios calculated from the material properties of the vessels show the potential for strong reflections as blood travels between certain sites within the circulation of alligators (Table 1). For example, substantial impedance mismatches caused by large increases in elastic modulus (E_{inc}) with very small changes in vessel cross-sectional area resulted in large reflection ratios between the right aorta and femoral and distal carotid arteries. Surprisingly, a small change in elastic modulus but large change in vessel area resulted in a large reflection ratio at the junction of the truncus and proximal right aorta. In contrast, limited reflections occurred between the distal right aorta and proximal carotid, allowing wave transmission into the periphery.

DISCUSSION

A number of observations indicate that wave reflections are present and prominent in the central circulation of alligators, including *1*) the substantial difference between the measured pressure and flow profiles in the right aorta, which are exaggerated during constriction but lessened during dilation (Figs.

Table 1. *E_{inc}, c_o, Z_c, and RR between vessels, calculated using material properties of central and peripheral blood vessels*

Vessel	Strain	E_{inc}, MPa	c_o, m/s	Z_c, MPa·s·m^{-3}	RR
TruncRA	0.55	0.387±0.043	3.95±0.16	12.9±0.61	] 0.67
RA_{Prox}	0.55	0.246±0.038	2.91±0.29	75.4±7.71	
RA_{Dist}	0.5	0.429±0.087	3.85±0.21	138±8.47	] 0.20
Car_{Prox}	0.5	0.338±0.16	3.71±0.44	211±25.1	] 0.57
Car_{Dist}	0.42	1.63±0.261	7.27±0.67	569±51.2	] 0.64
Femoral	0.28	1.66±0.182	7.41±0.39	1,278±61.7	

Values are means ± SE, and were determined by using a mean blood pressure of 5.5 kPa and associated physiological strain (see MATERIALS AND METHODS). E_{inc}, mean elastic modulus; c_o, pulse wave velocity; Z_c, characteristic impedance; RR, reflection ratio; TruncRA, junction of truncus and right aorta; RA_{Prox}, proximal right aorta; RA_{Dist}, distal right aorta; Car_{Prox}, proximal carotid artery; Car_{Dist}, distal carotid artery; Femoral, femoral artery. Specific locations of blood vessels are described in MATERIALS AND METHODS. RR between RA_{Dist} and Femoral was calculated assuming the femoral arteries present an impedance equivalent to two vessels in parallel.

2 and 6); *2*) the peaking of femoral pressure above aortic pressure in late systole/early diastole (Fig. 2), which can only be achieved through wave reflection effects (24); *3*) the significant effect of vasodilation on impedance phase (Fig. 4); *4*) the effects of dilation/constriction on the shapes of the aortic pressure and flow pulses (Fig. 6); *5*) the large modulus of the reflection coefficient (Fig. 5), particularly during constriction; *6*) the results of reflection analysis showing substantial reflected components of pressure and flow (Fig. 6); and *7*) the analysis of material properties of blood vessels showing marked impedance mismatches and large reflection ratios between several pairs of sites (Table 1). The relative shapes of the measured incident and reflected pressure and flow waves, the reflection effects, and the effects of dilation and constriction observed in the present study are generally similar to those observed in birds, dogs, ferrets, and humans (8, 16, 18, 19, 23, 24, 27, 37). Thus it is apparent that there are marked wave reflection effects in the central circulation of alligators and that the timing could potentially affect cardiac performance.

The magnitude of the reflected transients at the right aorta was considerable and was enhanced with constriction and reduced with dilation (Figs. 5 and 6). Furthermore, peripheral input impedance and pulse wave velocity increased with constriction and decreased with dilation (see RESULTS), as is typically reported in mammals (reviewed in Ref. 24). Thus, in alligators, changes in vascular tone appear to have altered both the magnitude of the reflections (via peripheral impedance) and the timing of their return (via pulse wave velocity), which in turn would affect the reflection coefficient and hence pressure and flow profiles in the aorta (28). In a similar fashion, the increased arterial stiffness and increased pulse wave velocity coincident with aging are responsible for changes in the magnitude and timing of reflections and the increased systolic pressure pulse in the mammalian ascending aorta (29), which would manifest as an increased global reflection coefficient at that site.

The reflections in alligators resulted in a prominent diastolic wave in the right aorta in both the control and dilated states and increased central systolic pulse pressure in control and constricted states (Fig. 6). If the primary benefit of appropriately timed wave reflections is the prolongation of the pressure and thus flow pulses with a limited change in the central pulse pressure (24), then the control state in alligators appears most effective in this regard (Fig. 6). Dilation resulted in such a large reduction in the magnitude of reflected waves that they made only a small contribution to extending the central pressure pulse. Conversely, constriction resulted in very large reflections that returned to the right aorta during late systole, so that central systolic pressure was increased markedly and the flow pulse was decreased markedly, neither of which are considered beneficial.

The material properties of the vessels predict that substantial reflections will occur as blood travels from the distal right aorta to the femoral arteries and distal carotid artery (Table 1). The presence of such reflections agrees with the reflection coefficients and blood flow patterns observed in the right aorta (Figs. 5 and 6), suggesting that much of the reflection appeared to originate in the periphery and that impedance mismatches are minimal in most of the more central circulation. However, the truncus, which serves as the root of the left ventricular outflow tract, was distinct from the proximal right aorta which it serves in having a lumen that was much larger (7.3-fold), appearing much like the bulbus in teleost fish or the aortic bulbus in whales. There was thus a large and abrupt impedance mismatch at the interface between the truncus and right aorta, and reflections should occur despite similar values of stiffness in these two vessels (Table 1). As a consequence of this anatomy, the pressure wavelength at the fundamental frequency was ~7.6 m (based on a heart rate of 0.5 Hz and a measured wave velocity of 3.8 m/s), which is 70 times longer than the truncus itself. Thus the time for the pressure wave to traverse the truncus is a negligible portion of the cardiac period, and the truncus should behave as a windkessel. This would reduce pulsatile pressures and flows in the more peripheral arteries (10, 16, 33) but also effectively isolate the heart from peripheral reflections.

As flow and pressure recordings demonstrated that there were substantial reflected waves in the right aorta just distal to the truncus (Fig. 6), this raises the intriguing possibility that the impedance mismatch between the truncus and right aorta functions to isolate the heart from these reflections. Such isolation may protect the heart from high pressures caused by reflections as observed during constricted states. Furthermore, crocodilians can raise their blood pressure to well over 100 mmHg when disturbed (personal observations of authors), which would be an enormous load at the heart if augmented by reflections.

There is also limited evidence that alligators may have the ability to control the extent of the impedance mismatch between the heart and right aorta. Force production of truncus strips increases and decreases up to 100% in response to epinephrine and vasoactive intestinal polypeptide, respectively (3). Thus, under adrenergic tone, the elastic modulus of the truncus would increase and the diameter would decrease so the impedance mismatch between the truncus and right aorta would be attenuated. If, under such conditions, the effect of the truncus in isolating the heart from the circulation was reduced so that the primary reflection site became the femoral arteries, then the fundamental wavelength of 7.6 m would be only 6 to 7 times longer than the distance from the heart to the major reflecting site (instead of 70-fold when the truncus is a major reflecting site). This is close to the optimum value of 4 for enhancement of cardiac function due to reflection effects (26) and may permit significant wave propagation effects to reach the heart in a beneficial manner.

The cross-sectional area and stiffness of blood vessels change along the arterial tree; thus pulse wave velocity calculated from the material properties of discrete arterial sections should differ in a predictable manner (lower than the mean in the central vessels and higher in the peripheral; see Table 1). With the use of pulse wave velocities from material properties (Table 1) and with the estimation that the proximal right aorta, distal right aorta and femoral artery comprise 20%, 70%, and 10% of the total length of the arterial tree (i.e., heart to femoral), respectively, the mean velocity along the entire tree was calculated to be 4.0 m/s. This value is almost identical to the measured value of 3.8 m/s under control conditions, which is also a mean value incorporating velocities from the distal right aorta to the femoral artery. This similarity, in combination with the similarity between the static reflection ratio between the distal right aorta and femoral arteries that was calculated from material properties (Table 1) and the mean reflection

coefficient at the right aorta that was calculated from blood flow and pressure (zero-order values average about 0.7), demonstrates a remarkable ability to predict reflection characteristics using only the material properties of the vessels.

In conclusion, like birds and mammals, alligators also possess a central arterial circulation with transmission line characteristics amenable to promoting significant wave reflection effects. Based on material properties of the vasculature, a major source of the reflections appears to originate near the femoral arteries. Substantial reflections (reflection coefficient up to 0.3) returned toward the heart during late systole/early diastole. Changes in peripheral impedance influenced the magnitude of the reflections and changes in pulse wave velocity altered the timing of their return. Unexpectedly, the heart itself appeared to be isolated from the arterial circulation by a large impedance mismatch at the junction of the truncus and right aorta. This isolation may protect the heart from elevated pressures in the central circulation that result from pronounced wave reflection effects in these large animals.

ACKNOWLEDGMENTS

We thank the animal care facilities staff at the University of British Columbia for care and handling of alligators.

Present address of M. H. Braun: Dept. of Zoology, Sidney Sussex College, Cambridge University, Sidney St., Cambridge CB2 3HU, UK.

GRANTS

This work was supported by Natural Sciences and Engineering Research Council Discovery Grants (to D. A. Syme and D. R. Jones).

REFERENCES

1. **Avolio AP, O'Rourke MF, Bulliman BT, Webster ME, and Mang K.** Systemic arterial hemodynamics in the diamond python *Morelia spilotes*. *Am J Physiol Regul Integr Comp Physiol* 243: R205–R212, 1982.
2. **Avolio AP, O'Rourke MF, and Webster ME.** Pulse-wave propagation in the arterial system of the diamond python *Morelia spilotes*. *Am J Physiol Regul Integr Comp Physiol* 245: R831–R836, 1983.
3. **Axelsson M and Franklin CE.** The calibre of the foramen of Panizza in *Crocodylus porosus* is variable and under adrenergic control. *J Comp Physiol [B]* 171: 341–346, 2001.
4. **Bergel DH.** The static elastic properties of the arterial wall. *J Physiol* 156: 445–457, 1961.
5. **Berger DS, Li JK, Laskey WK, and Noordergraaf A.** Repeated reflection of waves in the systemic arterial system. *Am J Physiol Heart Circ Physiol* 264: H269–H281, 1993.
6. **Braun MH, Brill RW, Gosline JM, and Jones DR.** Form and function of the bulbus arteriosus in yellowfin tuna (*Thunnus albacares*), bigeye tuna (*Thunnus obesus*) and blue marlin (*Makaira nigricans*): static properties. *J Exp Biol* 206: 3311–3326, 2003.
7. **Braun MH, Brill RW, Gosline JM, and Jones DR.** Form and function of the bulbus arteriosus in yellowfin tuna (*Thunnus albacares*): dynamic properties. *J Exp Biol* 206: 3327–3335, 2003.
8. **Burattini R and Campbell KB.** Comparative analysis of aortic impedance and wave reflection in ferrets and dogs. *Am J Physiol Heart Circ Physiol* 282: H244–H255, 2002.
9. **Fitchett DH.** LV-arterial coupling: interactive model to predict effect of wave reflections on LV energetics. *Am J Physiol Heart Circ Physiol* 261: H1026–H1033, 1991.
10. **Gibbons CA and Shadwick RE.** Circulatory mechanics in the toad *Bufo marinus*. II. Haemodynamics of the arterial windkessel. *J Exp Biol* 158: 291–306, 1991.
11. **Hayashi T, Nakayama Y, Tsumura K, Yoshimaru K, and Ueda H.** Reflection in the arterial system and the risk of coronary heart disease. *Am J Hypertens* 15: 405–409, 2002.
12. **Ina-Davies J and Struthers AD.** Pulse wave analysis and pulse wave velocity: a critical review of their strengths and weaknesses. *J Hypertens* 21: 463–472, 2003.
13. **Jones DR.** Cardiac energetics and the design of vertebrate arterial systems. In: *Efficiency and Economy in Animal Physiology*, edited by Blake RW. Cambridge, UK: Cambridge University Press, 1991, p. 159–168.
14. **Jones DR.** The crocodilian central circulation: reptilian or avian? *Verh Dtsch Zool Ges* 89: 209–218, 1996.
15. **Kassab GS.** Scaling laws of vascular trees: of form and function. *Am J Physiol Heart Circ Physiol* 290: H894–H903, 2006.
16. **Langille BL and Jones DR.** Dynamics of blood flow through the hearts and arterial systems of anuran amphibia. *J Exp Biol* 68: 1–17, 1977.
17. **Lantelme P, Mestre C, Lievre M, Gressard A, and Milon H.** Heart rate: an important confounder of pulse wave velocity assessment. *Hypertension* 39: 1083–1087, 2002.
18. **Laskey WK and Kussmaul WG.** Arterial wave reflection in heart failure. *Circulation* 75: 711–722, 1987.
19. **Li JK.** Time domain resolution of forward and reflected waves in the aorta. *IEEE Trans Biomed Eng* 33: 783–785, 1986.
20. **Milnor WR.** Aortic wavelength as a determinant of the relation between heart rate and body size in mammals. *Am J Physiol Regul Integr Comp Physiol* 237: R3–R6, 1979.
21. **Milnor WR.** *Hemodynamics.* Baltimore, MD: Williams & Wilkins, 1982.
22. **Mitchell GF, Pfeffer MA, Westerhof N, and Pfeffer JM.** Measurement of aortic input impedance in rats. *Am J Physiol Heart Circ Physiol* 267: H1907–H1915, 1994.
23. **Murgo JP, Westerhof N, Giolma JP, and Altobelli SA.** Aortic input impedance in normal man: relationship to pressure wave forms. *Circulation* 62: 105–116, 1980.
24. **Nichols WW and O'Rourke MF.** Wave reflections. In: *McDonald's Bloow Flow in Arteries: Theoretical, Experimental and Clinical Principles*. London: Arnold, 1998, p. 203–222.
25. **Nichols WW and Pepine CJ.** Left ventricular afterload and aortic input impedance: implications of pulsatile blood flow. *Prog Cardiovasc Dis* 24: 293–306, 1982.
26. **Noordergraaf A, Li JK, and Campbell KB.** Mammalian hemodynamics: a new similarity principle. *J Theor Biol* 79: 485–489, 1979.
27. **O'Rourke MF and Gallagher DE.** Pulse wave analysis. *J Hypertens Suppl* 14: S147–S157, 1996.
28. **O'Rourke MF and Kelly RP.** Wave reflection in the systemic circulation and its implications in ventricular function. *J Hypertens* 11: 327–337, 1993.
29. **O'Rourke MF and Mancia G.** Arterial stiffness. *J Hypertens* 17: 1–4, 1999.
30. **O'Rourke MF and Yaginuma T.** Wave reflections and the arterial pulse. *Arch Intern Med* 144: 366–371, 1984.
31. **Parker KH and Jones CJ.** Forward and backward running waves in the arteries: analysis using the method of characteristics. *J Biomech Eng* 112: 322–326, 1990.
32. **Segers P and Verdonck P.** Role of tapering in aortic wave reflection: hydraulic and mathematical model study. *J Biomech* 33: 299–306, 2000.
33. **Shelton G and Jones DR.** Pressure and volume relationships in the ventricle, conus and arterial arches of the frog heart. *J Exp Biol* 43: 479–488, 1965.
34. **Syme DA, Gamperl K, and Jones DR.** Delayed depolarization of the cog-wheel valve and pulmonary-to-systemic shunting in alligators. *J Exp Biol* 205: 1843–1851, 2002.
35. **Weber T, Auer J, O'Rourke MF, Kvas E, Lassnig E, Berent R, and Eber B.** Arterial stiffness, wave reflections, and the risk of coronary artery disease. *Circulation* 109: 184–189, 2004.
36. **Westerhof N and Noordergraaf A.** Errors in the measurement of hydraulic input impedance. *J Biomech* 3: 351–356, 1970.
37. **Westerhof N, Sipkema P, van den Bos GC, and Elzinga G.** Forward and backward waves in the arterial system. *Cardiovasc Res* 6: 648–656, 1972.
38. **Wilkinson IB, Mohammad NH, Tyrrell S, Hall IR, Webb DJ, Paul VE, Levy T, and Cockcroft JR.** Heart rate dependency of pulse pressure amplification and arterial stiffness. *Am J Hypertens* 15: 24–30, 2002.